Ultrasound in Med. & Biol., Vol. 37, No. 4, pp. 605–616, 2011

0301-5629/$ - see front matter

ELSEVIER

doi:10.1016/j.ultrasmedbio.2011.01.010

● *Original Contribution*

LEFT VENTRICULAR BORDER TRACKING USING CARDIAC MOTION MODELS AND OPTICAL FLOW

K. Y. Esther Leung,* Mikhail G. Danilouchkine,* Marijn van Stralen,*† Nico de Jong,*†‡ Antonius F. W. van der Steen,*† and Johan G. Bosch*

*Biomedical Engineering, Thoraxcenter, Erasmus MC, The Netherlands; †ICIN - Interuniversity Cardiology Institute of The Netherlands, Utrecht, The Netherlands; and ‡Physics of Fluids, University of Twente, Enschede, The Netherlands

(*Received* 26 *April* 2010; *revised* 14 *January* 2011; *in final form* 14 *January* 2011)

Abstract—The use of automated methods is becoming increasingly important for assessing cardiac function quantitatively and objectively. In this study, we propose a method for tracking three-dimensional (3-D) left ventricular contours. The method consists of a local optical flow tracker and a global tracker, which uses a statistical model of cardiac motion in an optical-flow formulation. We propose a combination of local and global trackers using gradient-based weights. The algorithm was tested on 35 echocardiographic sequences, with good results (surface error: 1.35 ± 0.46 mm, absolute volume error: 5.4 ± 4.8 mL). This demonstrates the method's potential in automated tracking in clinical quality echocardiograms, facilitating the quantitative and objective assessment of cardiac function. (E-mail: k.leung@erasmusmc.nl) © **2011 World Federation for Ultrasound in Medicine & Biology.**

Key Words: **Three-dimensional echocardiography, Optical flow, Principal component analysis, Tracking.**

INTRODUCTION

Echocardiography is a commonly used, safe and noninvasive technique that allows assessment of left ventricular (LV) function. Real-time three-dimensional (3-D) echocardiography, which has gained much interest in recent years, allows noninvasive imaging of the whole left ventricle in a few seconds. Compared with other modalities such as magnetic resonance imaging and computed tomography, images made with ultrasound may be more difficult to interpret. This is mainly due to the presence of speckle noise, as well as ultrasound artifacts that often lead to poorly visualized parts of the cardiac wall (see Fig. 1). Misinterpretation in these areas may lead to inaccuracies in quantification. This makes the automated analysis of such images generally more challenging.

Due to the large amount of 3-D data acquired, there is an increasing demand for automated methods to analyze LV functional parameters, such as LV volume, accurately and objectively. Therefore, segmentation and tracking in 3-D and four –dimensional (4-D) (3D+time) echocardiograms has gained considerable attention (Noble and Boukerroui 2006; Leung and Bosch 2010). Common automated methods include deformable models (Gérard et al. 2002; Montagnat et al. 2003; Walimbe et al. 2006; Nillesen et al. 2007), level sets (Corsi et al. 2002; Angelini et al. 2005), active appearance and active shape models (van Stralen et al. 2007; Hansegård et al. 2007a), state estimation (Orderud et al. 2007) and clustering/classification (Sanchez-Ortiz et al. 2002; Papademetris et al. 2001; Georgescu et al. 2005; Yang et al. 2008).

In recent years, efforts have shifted towards tracking methods for evaluating left ventricular dynamics. Tracking methods can be based on deformation of surfaces (Yan et al. 2007) or on tracking image intensities. Most commonly used intensity-based tracking techniques include nonrigid registration (Ledesma-Carbayo et al. 2005; Myronenko et al. 2007; Elen et al. 2008), Bayesian techniques (Papademetris et al. 2001), template/block matching (Yeung et al. 1998; Helle-Valle et al. 2005; Kawagishi 2008; Duan et al. 2008; Linguraru et al. 2008) and differential optical flow (Sühling et al. 2005; Veronesi et al. 2006). Many researched and commercialized methods (Leung and Bosch 2010) make use of knowledge contained in the image itself or impose general regularization constraints to provide smooth motion estimates. Compared with other modalities, tracking in ultrasound images is especially challenging, due to the presence of speckle patterns and

Address correspondence to: K. Y. Esther Leung, Biomedical Engineering, Thoraxcenter, Ee2302, Erasmus MC, P.O. Box 2040, 3000 CA Rotterdam, The Netherlands. E-mail: k.leung@erasmusmc.nl

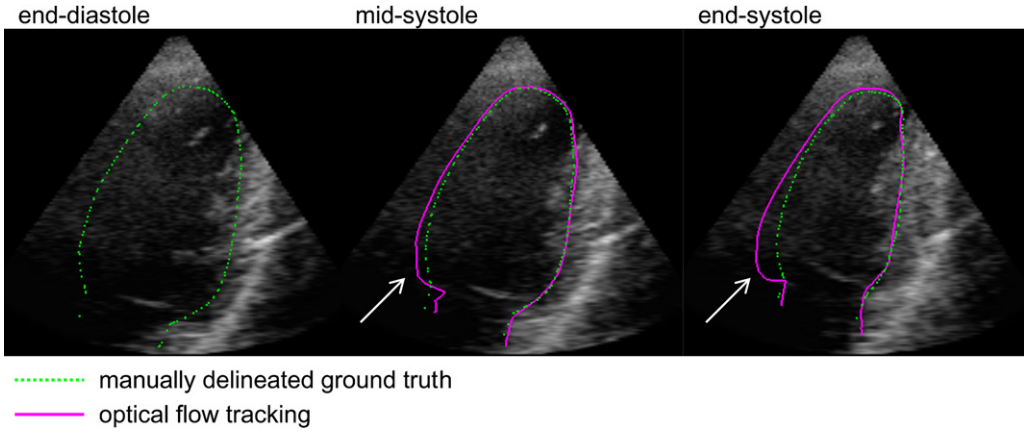

Fig. 1. Example of echocardiographic sequence (two-chamber view is shown), with poorly visualized cardiac wall in the anterior segments. Green dotted line denotes the manually delineated ground truth. Magenta solid line denotes optical flow tracking. Misinterpretation of the anterior wall (arrow) may lead to considerable inaccuracies in quantification.

ultrasound artifacts. It is our opinion that prior knowledge in the form of statistical modeling of cardiac motion will be of additional benefit for tracking left ventricular borders.

In this article, we aim at tracking the endocardial border through the cardiac cycle, given a manually delineated contour in end-diastole. Our proposed method is novel because it uses statistical modeling of cardiac motion as prior knowledge in a tracking framework. By using a statistical model, we incorporate realistic knowledge of cardiac function, derived from real patient data.

We make a distinction between spatial and temporal modeling of anatomical shape; this article addresses the latter aspect. In the medical imaging context, spatial variation is related to anatomical diversity across different patients, which can be used as priors in segmenting one 3-D image. Temporal variation captures the variability in an organ's shape due to physiologic activity. We use this knowledge to aid tracking throughout the cardiac cycle.

The proposed method consists of a *global* tracker which uses a *statistical model of cardiac motion* to ensure overall spatiotemporal consistency and a *local*, data-driven tracker for locally accurate tracking. We propose a combination, which emphasizes the advantages of each method: if the cardiac wall is obscured (see Fig. 1), we rely more on the global tracker, and if it is clearly visible, we rely more on the local tracker.

Previous work on optical flow

In this study, we choose to investigate optical flow. Optical flow based methods have previously been applied for motion analysis, modeling and tracking in ultrasound imaging. Most methods use the Horn-Schunck solution (Horn and Schunck 1981), which applies a global smoothness constraint on the motion field, or the Lucas-Kanade solution (Lucas and Kanade 1981), which assumes local motion consistency. For example, Mailloux et al. (1987) applied the Horn-Schunck solution to analyze two-dimensional (2-D) echocardiograms. Baraldi et al. (1996) compared three algorithms on synthesized ultrasound images and concluded that both Horn-Schunck and Lucas-Kanade approaches generated favorable results. LV wall motion was analyzed using the Lucas-Kanade method by Chunke et al. (1996). Mikić et al. (1998) first used optical flow for propagating contours throughout echocardiograms. Optical flow was used to initialize the contour in the subsequent frame, after which the actual contour detection was performed by active contours. More recently, Sühling et al. (2005) developed a combination of optical flow and b-splines for tracking in 2-D echocardiographic sequences. An application in 3-D echocardiography was described by Veronesi et al. (2006). In their paper, the Lucas-Kanade approach was used together with block matching to detect the long-axis of the left ventricle.

While optical flow has indeed been shown to be feasible in echocardiograms, it is important to realize that the method may fail if the structure to be tracked is poorly visible. This is often the case for clinical quality images; especially in 3-D, the large footprint of the transducer may hamper imaging between the ribs, causing considerable shadowing of the cardiac wall. In these areas, a plausible contour should be generated that is consistent with the expected cardiac motion and the remaining available image information. Statistical modeling provides an efficient way of modeling this cardiac motion.

Previous work on statistical modeling

Statistical modeling has been used in various ways for segmentation. Perhaps the most well known are those

based on active shape and active appearance models (Bosch et al. 2002; van Stralen et al. 2007; Hansegård et al. 2007b), which model typical shape and appearance variations in a patient population. These methods are effective in echocardiograms because they deliver plausible results, even when parts of the cardiac wall are poorly visualized. An interesting approach was described by Malassiotis and Strintzis (1999), who constrained an active contour-based segmentation by applying principal component analysis over the contour sequence at hand. Comaniciu et al. (2004) projected optical flow estimates back to the shape model space to generate a more robust segmentation. They used the mean shift method to combine multiple optical flow estimates. Hansegård et al. (2007a) proposed to estimate shape model parameters in a Kalman filtering approach, using estimates in the previous time-frames to generate new parameters for the current frame. Recently, Perperidis et al. (2007) suggested a segmentation method using registration with a shape model. This model was decoupled into two parts: interpatient statistics (spatial variations) and intrapatient statistics (temporal variations). The model parameters were numerically optimized in nonrigid-registration fashion, using a gradient-descent approach and a gradient-based similarity measure.

Goal and scope

In this article, we propose a combination of a *local* and a *global* tracker for tracking endocardial contours throughout the cardiac cycle. A novel aspect of this work is the integration of the statistical model for optical flow based tracking. The goal of the local tracker is to provide a locally accurate motion estimate by looking only at the data at hand, without using any (shape or motion) assumptions. The local tracker is based on differential optical flow. The goal of the global tracker is to ensure a global, spatiotemporally consistent result, in cases when the local tracking is unreliable (*e.g.*, due to poorly visualized cardiac wall). For the global tracker, statistical models of cardiac motion are integrated within the optical flow framework. The motion model is derived from manually delineated 4-D contours in *in vivo* images, resulting in a realistic modeling of cardiac wall motion.

Unlike most applications in ultrasound imaging (*e.g.*, Danilouchkine et al. 2008), we intend to use the optical flow method to track a large scale structure in the images, *i.e.*, the endocardial border, and not to track individual speckle patterns *e.g.*, to derive strain-related parameters. For the latter, a high frame rate is required, which is unavailable for current 3-D ultrasound imaging systems. Since we aim at estimating cardiac motion at this larger image scale, the tracking is performed in time-gain-compensated envelope data and not the raw radio-frequency data. The goal is to track endocardial contours throughout the cardiac cycle in this larger image scale, for quantification of volumes and ejection fractions.

METHODS

In this section, we explain the *local* and *global* trackers. Then, we describe the combination of these trackers using weights derived from intensity gradients.

Local tracker: optical flow

Optical flow tracking aims at finding the apparent motion (flow) of objects in an image sequence. The optical flow equation describes the relationship between the motion field ($\mathbf{v}$), the spatial ($\nabla I \equiv (\frac{\partial I}{\partial x}, \frac{\partial I}{\partial y}, \frac{\partial I}{\partial z}) = (I_x, I_y, I_z)$) and temporal gradient ($I_t = \frac{\partial I}{\partial t}$) in image intensity:

$$\nabla I(\mathbf{x}, t) \cdot v(\mathbf{x}, t) + I_t(\mathbf{x}, t) = 0, \tag{1}$$

where $\mathbf{x}$ denotes spatial coordinates and t denotes time. $\mathbf{v}$ consists of the velocity components of the motion field; for 3-D images, $\mathbf{v} = (v_x(\mathbf{a}), v_y(\mathbf{a}), v_z(\mathbf{a}))$. Each velocity component can be described with k parameters $\mathbf{a}$, to denote different types of velocity models (*e.g.*, translation-only, similarity, or affine).

To solve eqn (1) for $\mathbf{v}$, more assumptions are required because this one equation contains k unknowns. The commonly-used Lucas-Kanade approach assumes that the velocity is constant in a small region B around $\mathbf{x}$. The velocity vector can then be resolved with least-squares. A sum-of-squares error term is set up as follows (Lucas and Kanade 1981):

$$\varepsilon = \sum_{x \in B} (w(\mathbf{x}))^2 [\nabla I(\mathbf{x}) \cdot v + I_t(\mathbf{x})]^2, \tag{2}$$

where w represents a local weight. For a translation-only description of $\mathbf{v}$, this can be solved by differentiating eqn (2) with respect to each translation component $\mathbf{v} = (v_x, v_y, v_z)$, and equating the result to zero. This leads to the following system of equations (note that w, I_u, I_v and I_t depend on $\mathbf{x}$):

$$\begin{aligned} &\mathbf{R}\mathbf{v} = \mathbf{e}, \text{ with } R_{uv} = \sum_{x \in B} w^2 I_u I_v, \text{ and} \\ &e_u = -\sum_{x \in B} w^2 I_t I_u \text{ for } u, v = x, y, z. \end{aligned} \tag{3}$$

By applying the local tracker frame-by-frame at the contour locations, the end-diastolic contour can be propagated throughout the whole sequence.

Global tracker: statistical modeling and optical flow

The global tracker is an embedding of statistical models of cardiac motion in the optical flow formulation.

First, the training of the statistical motion models is described. Then, we explain the integration of the model with the optical flow equation. This is followed by some implementation details.

Motion modeling. The motion models are trained using contours of *in vivo* data sets. These contours are represented by the 3-D coordinates of points which are evenly distributed on the endocardial surface. We chose to model the cardiac motion on a frame-to-frame basis, using *affine transforms*. Principal component analysis (PCA) is used to generate a compact representation of these transforms. Note that our approach is different from traditional statistical shape models (Cootes et al. 2001), which describe the statistical variation of the shape using the actual contour points themselves. Instead, we model the motion using affine parameters that are extracted from the training contours, and apply PCA to these parameters.

Furthermore, for a time-continuous result, we take into account the motion of the whole cardiac cycle in one model. The frame-to-frame motion is represented by one affine transform. Although this may seem a rather tight restriction, we anticipate that this representation will have a small error because of limited differences between two consecutive frames. We choose to model only the global motion this way and will further refine the tracking using the local tracker.

The affine transforms allows the modeling of translation, rotation, shear and scaling, represented by 12 parameters:

$$\mathbf{v}=\begin{pmatrix} v_x \\ v_y \\ v_z \end{pmatrix}=\begin{pmatrix} a_{x0} & a_{x1} & a_{x2} \\ a_{y0} & a_{y1} & a_{y2} \\ a_{z0} & a_{z1} & a_{z2} \end{pmatrix}\begin{pmatrix} x \\ y \\ z \end{pmatrix}+\begin{pmatrix} a_{x3} \\ a_{y3} \\ a_{z3} \end{pmatrix}. \quad (4)$$

These affine parameters are obtained using Procrustes analysis (Gower 1975). First, all end-diastolic training contours are aligned to a common coordinate system. This is necessary to remove acquisition (spatial) variations between patients, as we are interested in the functional (temporal) variations. This step resembles what is also done in multi-view active appearance models (Bosch et al. 2002), in which Procrustes analysis is used to align all input shapes, to eliminate variations in acquisition that are not related to anatomical variations. After this step, the found alignment transform for each end-diastolic contour is applied to the rest of the sequence, so that the whole sequence is in this common coordinate system.

Next, Procrustes analysis is applied between consecutive frames of the sequence to extract the frame-to-frame affine transforms. For each contour sequence, the 3-D affine modeling of F cardiac phases results in 12* (F-1) parameters. These are concatenated into a column vector $\mathbf{a}$ and are the inputs to the PCA:

$$\mathbf{a}=\left(a_{x0}^1, a_{x1}^1, \ldots a_{z3}^1, a_{x0}^2, \ldots, a_{x0}^{F-1}, \ldots, a_{z3}^{F-1}\right)^T, \quad (5)$$

where ^{T} denotes vector transpose. PCA gives a compact description of the motion variations by reducing the dimensionality of the input affine transforms (Cootes et al. 2001). This allows us to approximate a set of affine transforms $\mathbf{a}$ throughout the cardiac cycle using the average transform $\bar{\mathbf{a}}$, the PCA eigenvectors $\mathbf{\Phi}$ and the PCA parameters $\mathbf{c}$:

$$\mathbf{a}\approx\bar{\mathbf{a}}+\mathbf{\Phi}\,\mathbf{c}. \quad (6)$$

Since the eigenvectors are sorted in order of variance, modes with low variance can be removed easily by truncating $\mathbf{c}$ and $\mathbf{\Phi}$. The remaining k modes will then encompass only a proportion g of the total variation G:

$$\sum_{i=1}^{k}\lambda_i \geq gG, \text{ with } G=\sum_{i=1}^{p}\lambda_i, \quad (7)$$

where p is the total number of modes and λ_i denotes the i^{th} eigenvalue (Mitchell et al. 2002). With formula (6), the frame-to-frame affine transform throughout the cardiac cycle is described by k parameters $\mathbf{c}$, which are to be solved here *via* optical flow. For this study, g = 95% is used, corresponding with k = 24 PCA parameters for a model built with 35 contours.

Integration with optical flow. For tracking in a new image sequence, the trained statistical model is integrated into the optical flow equation. In essence, the statistical model is used as the underlying assumption to solve eqn (1). Each affine component a_j^f [formula (4)] of a certain cardiac phase f can be described with $\mathbf{c}$, the corresponding row of $\mathbf{\Phi}$ and the corresponding component of $\bar{\mathbf{a}}$:

$$a_j^f=\bar{\mathbf{a}}_j^f+\mathbf{\Phi}_j^f\ \mathbf{c}. \quad (8)$$

This is substituted in each affine component in formula (4) and this in turn is substituted in eqn (1). This leads to the modified optical flow equation:

$$\begin{aligned} E(\mathbf{x},t)&=I_t+I_x\bar{\mathbf{a}}_x+I_y\bar{\mathbf{a}}_y+I_z\bar{\mathbf{a}}_z \\ &+\left(I_x\mathbf{\Phi}_x+I_y\mathbf{\Phi}_y+I_z\mathbf{\Phi}_z\right)\mathbf{c}=0 \end{aligned} \quad (9)$$

where $\bar{a}_d=x\bar{a}_{d0}^f+y\bar{a}_{d1}^f+z\bar{a}_{d2}^f+\bar{a}_{d3}^f$
and $\mathbf{\Phi}_d=x\mathbf{\Phi}_{d0}^f+y\mathbf{\Phi}_{d1}^f+z\mathbf{\Phi}_{d2}^f+\mathbf{\Phi}_{d3}^f$
for $d=x,y,z$.

The objective is to find $\mathbf{c}$, given the spatial gradients I_x, I_y, I_z and temporal gradient I_t. A solution is to constrain the equation by assuming that the parameters $\mathbf{c}$ are constant in all regions around the contour and all cardiac phases, similar to the Lucas-Kanade approach [formula (2)]. We can then set up a sum-of-squares error term ε_{total}:

$$\varepsilon_{total} = \sum_{\mathbf{x}} \sum_{f} [E(\mathbf{x}, f)]^2. \tag{10}$$

By differentiating ε_{total} to each element in $\mathbf{c}$ and setting this to zero, a system of linear equations is obtained, similar to eqn (3):

$$\mathbf{Rc} = \mathbf{e}, \tag{11}$$

where $\mathbf{R}$ is a k-by-k symmetrical matrix, and $\mathbf{c}$ and $\mathbf{e}$ are k-by-1 vectors:

$$\begin{aligned} R_{uv} &= \sum_{\mathbf{x}} \sum_{f} w^2 \left(I_x \phi_x^u + I_y \phi_y^u + I_z \phi_z^u \right) \\ &\quad \left(I_x \phi_x^v + I_y \phi_y^v + I_z \phi_z^v \right) \\ e_u &= - \sum_{x} \sum_{f} w^2 \left(I_t + I_x \bar{a}_x + I_y \bar{a}_y + I_z \bar{a}_z \right) \\ &\quad \left(I_x \phi_x^u + I_y \phi_y^u + I_z \phi_z^u \right) \end{aligned} \tag{12}$$

where $\mathbf{\Phi}_d^u$ is the u^{th} element of $\mathbf{\Phi}_d^f$, the row in the eigenvector matrix corresponding with phase f (note that all terms depend on $\mathbf{x}$).

Implementation details. In practice, the algorithm needs a 3-D contour of the end-diastolic (ED) frame as a starting point for tracking in a new image. Here, the manually delineated ED contour is taken. The weight w in formula (12) was 1 if the voxel was inside the transducer's imaging sector and 0 otherwise, to prevent the influence of the image sector borders on tracking. The ED contour of the new image was first transformed to the common coordinate system using Procrustes analysis, in concordance with the model training step. The pseudocode in Table 1 lists the steps for resolving the tracking parameters.

Combination: gradient-based weights

In vivo echocardiograms often suffer from occlusions: parts of the cardiac wall can be invisible due to drop-out (when the imaged structure is parallel to the ultrasound beam), shadowing (when objects in the ultrasound path causes high reflections or attenuation) or low signal-to-noise ratio. In 3-D echocardiography, this is particularly apparent in the anterior wall (Nemes et al. 2007). In these areas, we would like to rely on the overall plausible solution of the global tracker. In areas where the structures are clearly visible (*e.g.*, the septal wall, the mitral valve ring), we would like to rely on the local tracker, to give a locally accurate result. These clearly visible structures usually have a high intensity gradient near the endocardial border.

Table 1. Global tracking scheme

(A) For each image pair f:
  (1) calculate spatial and temporal derivatives
  (2) populate formula (12) using derivatives of frame pair f
(B) Solve eqn (11) for $\mathbf{c}$
(C) Convert $\mathbf{c}$ into affine parameters $\mathbf{a}$ [formula (6)]
(D) Apply $\mathbf{a}$ to ED contour frame-by-frame

The combined result is determined by transforming the ED contour frame-by-frame, using weighed results of the local and global trackers. Each point on the contour is transformed to coordinates $\mathbf{x}_{combined}$, determined by weighing the results of the local tracking ($\mathbf{x}_L$) and the global method ($\mathbf{x}_G$) as follows:

$$\mathbf{x}_{combined}^f = \beta \mathbf{x}_L^f + (1-\beta)\mathbf{x}_G^f. \tag{13}$$

β is a local weight based on the local gradient norm $|\nabla I|$ of the 4-D image sequence:

$$\beta(\mathbf{x}) = \left(\frac{|\nabla I| - |\nabla I|_{min}}{|\nabla I|_{max} - |\nabla I|_{min}} \right)^2, \tag{14}$$

where $|\nabla I|_{min}$ was the minimum and $|\nabla I|_{max}$ was the maximum gradient norm in the whole image. The quadratic function is used so that the local tracker will be preferred only for relatively high gradients; this had a better performance than a linear function in initial tests.

Experimental details

Data. To test the performance of the proposed segmentation method, images were acquired of the left ventricle in patients referred for stress echocardiography. Only images obtained in the rest stage were analyzed. Data of 35 patients were acquired with a Philips Sonos 7500 system (Philips Medical Systems, Best, The Netherlands), equipped with a X4 matrix array transducer. Typical spatial dimensions were 160 × 144 × 208 voxels with 1 mm × 1 mm × 0.7 mm resolution. The 3-D data set was comprised from four electrocardiographically gated pyramidal subvolumes. Twenty of these patients underwent coronary angiography: six patients had no significant vessel disease, eight patients had one-vessel disease (two in the left-anterior-descending [LAD] coronary artery region, four in the right-coronary-artery [RCA] region, two in the left-circumflex-artery [LCX] region), three patients had two-vessel disease (LCX and RCA, LAD and RCA, LAD and LCX) and three patients had three-vessel disease. The institutional review board approved the study and all patients gave informed consent.

Contour delineation as ground truth. For training the motion model and for validating the tracking algorithm, gold standard contours were needed. Full-cycle endocardial borders were drawn with a previously developed semiautomated method, based on pattern matching and dynamic programming (van Stralen et al. 2005). In short,

the contour was delineated in the four-chamber and two-chamber views in end-diastole and end-systole. End-diastole was determined by the R-peak of the ECG, end-systole was defined as the frame before the opening of the mitral valve, which was determined visually. These anatomical views were selected manually by indicating the apex, the mitral valve and the direction of the four-chamber in the end-diastolic 3-D image (Leung et al. 2008). The two-chamber cross-section is defined as the view perpendicular to the four-chamber, passing through the long-axis, with the long-axis defined as the line passing through the apex and the mitral valve center. Dynamic programming was used to detect the entire 3-D surface, aided by the intensity patterns along the user-delineated contours. The detected borders were evaluated visually in 10 long-axis cross-sections at 18 degrees increment in all cardiac phases. If needed, the detected contours were manually corrected to ensure temporal coherence. This method produced accurate contours that were previously validated by MRI on a different set of data in a previous study (van Stralen et al. 2005). Three-dimensional points were sampled on the delineated surface at equidistant angles and short-axis levels to provide an even distribution of points, according to van Stralen et al. (2005).

Evaluation. Tracking was performed using the local tracker, the global tracker and their combination. Motion models were built in a leave-one-out fashion: 34 contours were used to build the model and the trackers were tested on the remaining image; this is then repeated for all the images. As mentioned before, we made a distinction between segmentation in one image and tracking throughout the cardiac cycle and the objective of this article is to evaluate the performance of the tracking. Therefore, we used the delineated contour of the (first) end-diastolic frame as initialization for the tracker.

Errors were calculated with respect to the ground truth. Surface errors are calculated symmetrically by taking the Euclidean distance between a point of the result contour and its projection on the true contour, and vice versa (Van Ginneken et al. 2006). Ejection fraction was defined as: $EF=(V_{ED}-V_{ES})/V_{ED}$, where V_{ED} is the end-diastolic volume and V_{ES} the end-systolic volume. Regression analysis was performed following Bland and Altman (1986). Statistical testing was performed using the paired t-test.

RESULTS

Figure 2 shows the main modes of variation captured in a model built with 35 contours. The main contraction-expansion pattern can be seen in the average transform [$\bar{\mathbf{a}}$, formula (4)]. An example of local, global, and combined tracking results can be seen in Figure 3. This figure shows

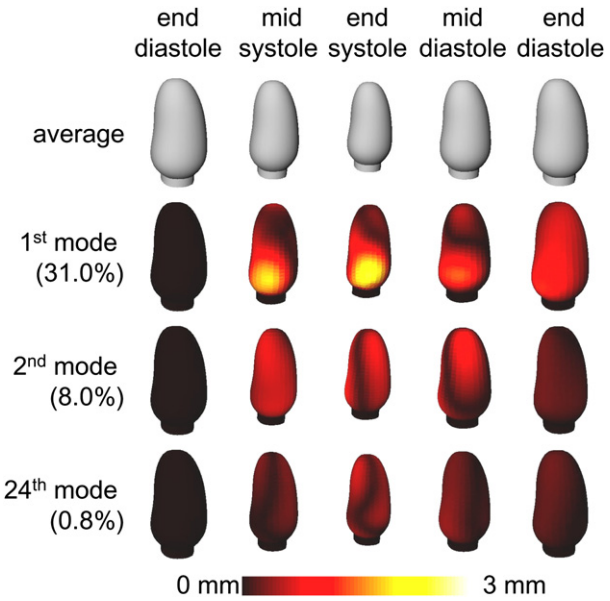

Fig. 2. Eigenvariations (three standard deviations) of the first, second and 24th mode of the motion model, with the corresponding amount of variation λ/G [see formula (7)], built with 35 contours. The variation with respect to the average motion in terms of surface distances is color coded onto the surfaces.

qualitatively the merit of combining the local and global trackers: for obscured cardiac wall in the anterior segments, the global tracker is used, whereas if the cardiac wall is clearly visible, the local tracker takes over.

Figure 4 shows the local surface errors in bull's eye plots, following standard protocol of the American Heart Association (Cerqueira et al. 2002). These quantitative results corroborate the qualitative results of Figure 3: in the anterior segments, the global tracker gives spatiotemporally consistent results that are better than that of the local tracker. The combined method takes this into account accordingly.

Figures 5 and 6 show the average ground truth volumes and the tracking results as a function of the cardiac cycle. The overall tracking errors are summarized in Table 2. Figure 7 shows the results of the regression analysis of the volume errors. The manually defined ED volume is omitted from this regression analysis. The combined tracker produces the lowest surface and volume errors.

DISCUSSION

In this study, we proposed methods for tracking the endocardial contours in 3-D echocardiographic sequences. The combination of the local and global trackers gave the best results (Fig. 4, Table 2). The global tracker gave realistic result based on the statistical

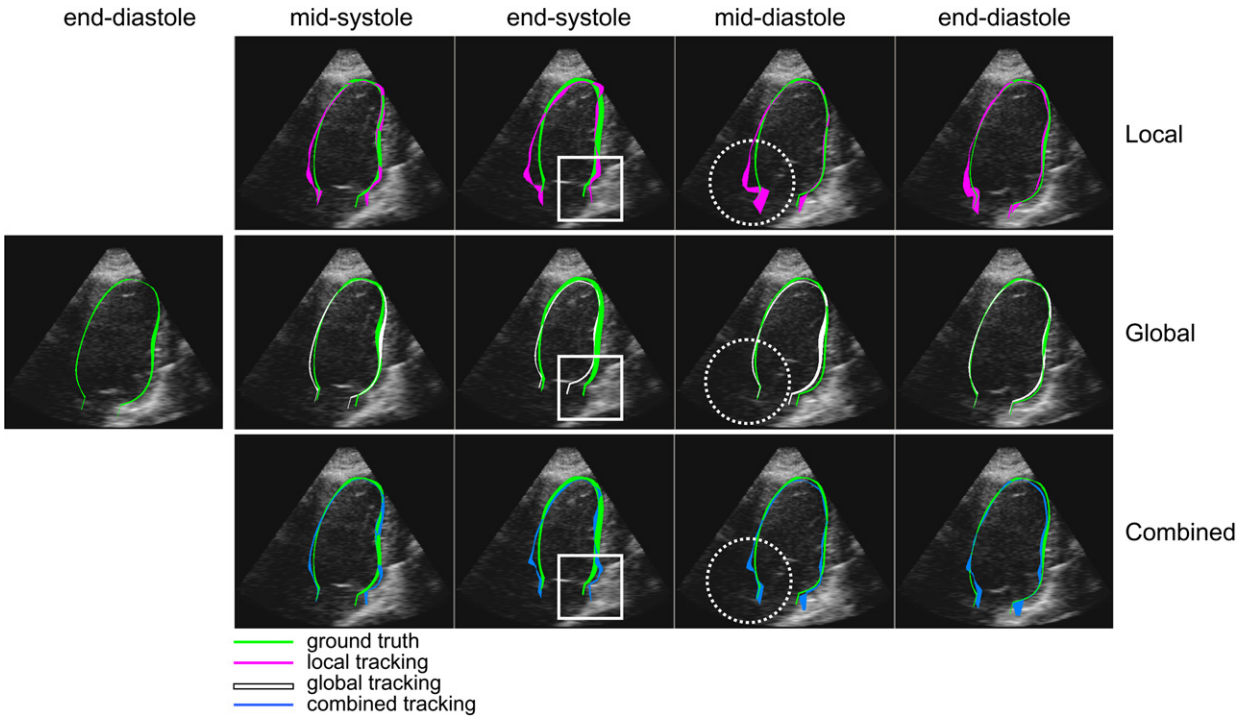

Fig. 3. Tracking using the local tracker (magenta line), global tracker (white line) and both methods combined (blue line). The two-chamber cross-section is shown. Green line denotes the ground truth. Solid square: for clearly visible structures, the local tracker is more accurate than the global tracker. Dotted circle: for obscured cardiac wall, poor local tracking is compensated by the global tracking in the combination.

modeling of cardiac motion; whereas the local tracker was accurate when the structures are clearly visible, *e.g.*, in the inferoseptal region. However, in the anterior segments, the local tracker was problematic.

In a previous study, our clinical partners analyzed 36 rest and stress Sonos 7500 (Philips Medical Systems) datasets visually and scored each of the 17 segments as 4 = excellent quality without possibility to improve, 3 = good quality without artifacts, 2 = sufficient quality without artifacts or good quality with artifacts, 1 = poor or moderate quality with artifacts and 0 = nonvisualized (Nemes et al. 2007). In the rest images, the anterior segments received a score 0 in 12 out of 36 patients and a score 1 in six out of 36 patients. This corroborates the findings in our study: in anterior segments, the global tracker gave spatiotemporally consistent contours, which were especially useful in areas with poorly visualized cardiac wall. Although the image quality has improved

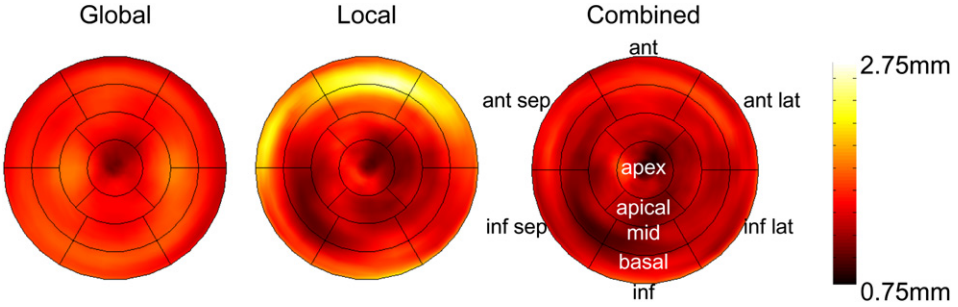

Fig. 4. Local surface errors, color-coded on bulls eye plots, averaged over all patients and cardiac phases. Notice the improvement in the anterior region using the combined method, corresponding to better tracking in the anterior region which typically has poorly visualized cardiac wall.

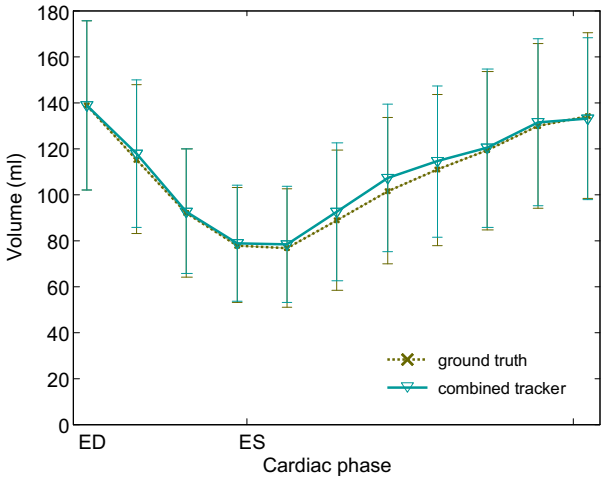

Fig. 5. Ground truth volume and the results of the combined tracker as a function of cardiac phase.

with the newer ultrasound imaging systems, drop-out is still an issue in *e.g.*, obese patients or patients with enlarged ventricles.

From Table 2, it is apparent that the local tracker had slightly worse results in diastole than in systole. Because the local tracker was performed on a frame-to-frame basis, errors could accumulate across the cardiac cycle. On the other hand, the global tracker is inherently spatio-temporally coherent because it models the entire cardiac cycle. This finding can be used to adjust the weights of the combined method to rely more on the global tracking near the end of the cardiac cycle. Also, it is possible to add an extra backtracking step for the local tracker (from the last image frame to the first), to further reduce the accumulation of errors.

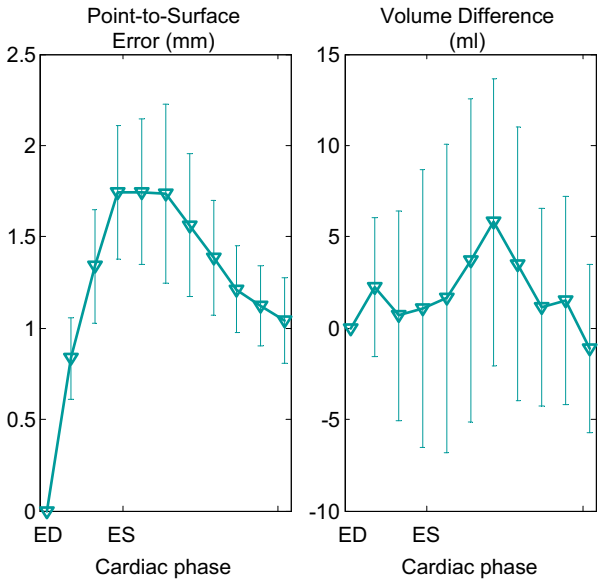

Fig. 6. Errors of the combined tracker as a function of cardiac phase.

In Table 2, we report both signed and absolute volume and ejection fraction errors. The average values of the signed (V and EF) errors show that there is hardly any bias in the errors. The absolute errors [abs(V) and abs(EF)] show that the errors are quite small. The standard deviation of the signed (V and EF) errors may seem significant compared with the average. However, our results compare quite favorably with those reported in literature (Table 3).

Comparison with other work

Table 3 lists results of segmentation and tracking algorithms, reported in literature. Due to the vast amount of literature, the scope of our comparison is constrained to the most recent works on 3-D cardiac ultrasound, with surface or volume errors reported. Furthermore, comparisons with papers on strain analysis are omitted, as no strain results were available with our method. A distinction was made between segmentation and tracking methods, as ours is a tracking method.

The errors obtained in this study compare favorably with the ones reported in the previously published papers. However, since ours is a tracking method and needs a 3-D initialization, the errors cannot be entirely compared with those of the segmentation-only papers. A second comment is that the methods of Myronenko et al. (2007) and Duan et al. (2008) were evaluated on open chest animal models in which the cardiac wall in most cases is clearly visible (which is not the case with *in vivo* human data).

Several papers have been published on block matching vs. optical flow. Malpica et al. (2004) compared block-matching and the Lucas-Kanade approach and concluded that the latter was best for contrast echocardiograms. Veronesi et al. (2006) used both methods consecutively to detect the long-axis of the left ventricle in echocardiographic sequences. Combinations of smart block-matching (Behar et al. 2004; Linguraru et al. 2008) and optical flow may be used to further refine the trackers.

Limitations and extensions

An inherent limitation of model-based methods is that the training sets should comprise the expected variation of the underlying anatomical function. To demonstrate the versatility of the proposed approach, the image data included a mixed population of normal and abnormal heart function. Still, good results were obtained in this study, despite this large variability.

Although we have shown favorable results with respect to other methods reported in literature, it is no

Table 2. Average ± standard deviation of tracking errors, also separated into systolic and diastolic values

	S	*V*	abs(*V*)	EF	abs(EF)
	mm	mL	mL	%	%
Overall					
Local	1.52 ± 0.54	3.8 ± 8.1	6.9 ± 5.7	4.8 ± 6.5	6.3 ± 5.1
Global	1.51 ± 0.69	−2.0 ± 10.0	7.6 ± 6.8	−1.9 ± 6.7	5.4 ± 4.3
Combined	1.35 ± 0.46*†	1.9 ± 6.9	5.4 ± 4.8*†	1.2 ± 5.7	4.7 ± 3.4*
Systole					
Local	1.47 ± 0.63†	3.8 ± 7.2	6.2 ± 5.3		
Global	1.56 ± 0.73	0.8 ± 7.9	6.2 ± 4.9		
Combined	1.28 ± 0.53*†	1.4 ± 6.0	4.6 ± 4.0*†		
Diastole					
Local	1.55 ± 0.47	3.8 ± 8.6	7.3 ± 5.9		
Global	1.48 ± 0.66*	−3.6 ± 10.7	8.4 ± 7.6*		
Combined	1.39 ± 0.42*†	2.2 ± 7.4	5.8 ± 5.1*†		

S = surface; *V* = volume; abs(*V*) = absolute volume; EF = ejection fraction; abs(EF) = absolute EF.
* Statistically significantly smaller ($p < 0.05$) than the local tracker.
† Statistically significantly smaller than the global tracker.

easy task to establish the clinical relevance of the proposed method. An appropriate manually delineated standard is very difficult to define, due to inter- and intra-observer variabilities. The clinical reference standard for left ventricular volume estimation is magnetic resonance imaging (MRI). A comparison with MRI volumes is unfortunately unavailable for the data in this study. When comparing these modalities, one should keep in mind that differences in imaging principle cause discrepancies in spatiotemporal resolution and in the visualization of trabecular structures. This has led to a general underestimation of left ventricular volumes by echo (Leung and Bosch 2010). An independent, realistic dynamic standard is still lacking to thoroughly establish the accuracy of segmentation and tracking methods in general.

For a more detailed look at the differences between tracking in normal and abnormal sequences, one would have to obtain many more patients in all kinds of pathologies, for example in an extensive clinical trial. Previously, we have performed feasibility studies on classifying localized pathologies in echocardiographic sequences using statistical shape models (Bosch et al. 2005; Leung and Bosch 2008). However, the datasets for building and validating the model in these studies were considerably larger. Moreover, the models represented only 2-D motion. Therefore, the question about the suitability of the proposed approach for the purposes of classification of the local heart abnormalities remains open and definitely requires further investigation. We anticipate that building separate models for different pathologies can further improve the results; in that case, the best performing model (*e.g.*, with the lowest intensity tracking error) can be taken as the final result.

The focus of this article is on tracking of the left ventricular borders; as such the proposed tracking method needed an initialization in the first image frame. In the future, this can be replaced by an automated 3-D segmentation algorithm. We have had promising results with the active appearance model method, which uses a statistical model of the anatomy in a single frame (*e.g.*, end-diastole) (Leung et al. 2010). We think that the combination of this method and the proposed tracker will give a fully automated solution, which incorporates statistical modeling of both anatomy and function. This is a subject of further investigation.

The proposed method distinguishes itself by modeling cardiac motion statistics, applied to tracking of contours. The role of cardiac modeling has yet to be proven for other applications, such as speckle tracking to evaluate *e.g.*, strain. We believe that the promising results in this study encourage us to investigate this further for other applications. For example, the proposed method may be used as a more accurate initialization for frame-to-frame speckle tracking. Alternatively, in the clinical setting the user may select the relevant pathological model to achieve a better accuracy.

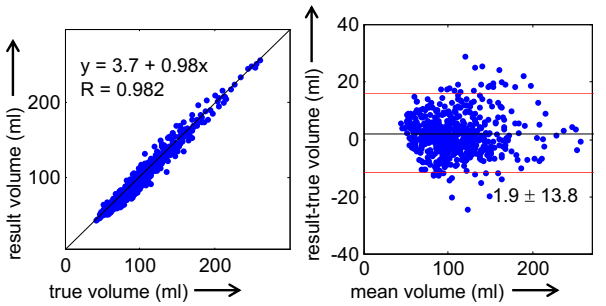

Fig. 7. Regression and limits-of-agreement analysis of the combined tracker.

Table 3. Comparison with cardiac ultrasound 4-D segmentation and tracking methods from literature

		S	*V*	abs(*V*)	EF	abs(EF)
Publication	*N*	mm	mL	mL	%	%
Segmentation only						
Angelini et al. (2001)	6		ED: −3.9 ± 20.2 ES: −9.1 ± 8.7	ED: 13.9 ± 14.0 ES: 9.9 ± 7.6	8.8 ± 5.6	8.8 ± 5.6
Corsi et al. (2002)	25		−15.6 ± 20.6 (ED and ES only)			
Sanchez-Ortiz et al. (2002)	14		6.6 ± 37.1			
Wolf et al. (2002)	20	3.44 ± 1.18				
Lin et al. (2003)	24	1.64 ± 0.50				
Angelini et al. (2005)	10		ED: 16.1 ± 25.6 ES: 6.6 ± 17.5	ED: 21.4 ± 20.8 ES: 10.6 ± 15.3	0.6 ± 11.3	10.0 ± 4.1
Walimbe et al. (2006)	5			ED: 8.0 ± 1.87 ES: 8.8 ± 2.39		7.2 ± 0.84
Hansegård et al. (2007a)	36	3.4 ± 2.3	ED: –3.1 ± 20 ES: 0.61± 13		−1.3 ± 6.3	
Zhu et al. (2007)	22	1.45 ± 0.30				
Segmentation and tracking						
Zagrodsky et al. (2005)	10		ED: 17.5 ± 11 ES: 9.8 ± 10.8		7.6 ± 5.5	
Hansegård et al. (2007b)	21	2.2 ± 0.56	3.4 ± 10		−7.7 ± 6	
Orderud et al. (2007)	21	2.7	4.1 ± 12.6			
Tracking only						
Myronenko et al. (2007)	1*	1.03 ± 0.62				
Duan et al. (2008)	40†			3.9 ± 2.5		
Yang et al. (2008)	31	1.28	1.11			
Current method						
Combined	35	1.35 ± 0.46	1.9 ± 6 .9	5.4 ± 4.8	1.2 ± 5.7	4.7 ± 3.4

N denotes the number of subjects. Average ± standard deviation of surface *S*, volume *V*, absolute volume abs(*V*), ejection fraction (EF) and absolute ejection fraction [abs(EF)] errors. Empty columns mean that data were not available.

* One open chest pig, 10 scans.

† Open chest dogs.

CONCLUSION

A method for tracking contours in 3-D+time left ventricular echocardiograms was proposed. The method consists of a local optical flow tracker and global tracker, which uses a model of cardiac motion in an optical-flow based formulation. We proposed a combination of local and global trackers using gradient-based weights. Good estimates of left ventricular volume and ejection fraction were obtained. This shows the feasibility of the method for tracking in clinical quality echocardiograms, facilitating the quantitative and objective assessment of functional parameters.

Acknowledgments—This research is supported by the Dutch Technology Foundation STW (grant 06666), applied science division of NWO and the Technology Program of the Ministry of Economic Affairs, The Netherlands.

REFERENCES

Angelini ED, Homma S, Pearson G, Holmes JW, Laine AF. Segmentation of real-time three-dimensional ultrasound for quantification of ventricular function: A clinical study on right and left ventricles. Ultrasound Med Biol 2005;31:1143–1158.

Angelini ED, Laine AF, Takuma S, Holmes JW, Homma S. LV volume quantification *via* spatiotemporal analysis of real-time 3D echocardiography. IEEE Trans Med Imaging 2001;20:457–469.

Baraldi P, Sarti A, Lamberti C, Prandini A, Sgallari F. Evaluation of differential optical flow techniques on synthesized echo images. IEEE Trans Biomed Eng 1996;43:259–272.

Behar V, Adam D, Lysyansky P, Friedman Z. Improving motion estimation by accounting for local image distortion. Ultrasonics 2004;43: 57–65.

Bland JM, Altman DG. Statistical methods for assessing agreement between two methods of clinical measurement. Lancet 1986;327: 307–310.

Bosch JG, Mitchell SC, Lelieveldt BPF, Nijland F, Kamp O, Sonka M, Reiber JHC. Automatic segmentation of echocardiographic sequences by active appearance motion models. IEEE Trans Med Imaging 2002;21:1374–1383.

Bosch JG, Nijland F, Mitchell SC, Lelieveldt BPF, Kamp O, Reiber JHC, Sonka M. Computer-aided diagnosis via model-based shape analysis: Automated classification of wall motion abnormalities in echocardiograms. Acad Radiol 2005;12:358–367.

Cerqueira MD, Weissman NJ, Dilsizian V, Jacobs AK, Kaul S, Laskey WK, Pennell DJ, Rumberger JA, Ryan T, Verani M. Standardized myocardial segmentation and nomenclature for tomographic imaging of the heart. Circulation 2002;105:539–542.

Chunke Y, Terada K, Oe S. Motion analysis of echocardiograph using optical flow method. Proc IEEE Int Conf Systems Man Cybernetics 1996;1:672–677.

Comaniciu D, Zhou XS, Krishnan S. Robust real-time myocardial border tracking for echocardiography: An information fusion approach. IEEE Trans Med Imaging 2004;23:849–860.

Cootes TF, Edwards GJ, Taylor CJ. Active appearance models. IEEE Trans Pattern Anal Mach Intell 2001;23:681–685.

Corsi C, Saracino G, Sarti A, Lamberti C. Left ventricular volume estimation for real-time three-dimensional echocardiography. IEEE Trans Med Imaging 2002;21:1202–1208.

Danilouchkine MG, Mastik F, van der Steen AFW. Accuracy in prediction of catheter rotation in IVUS with feature-based optical flow–A phantom study. IEEE Trans Inf Technol Biomed 2008;12:356–365.

Duan Q, Angelini ED, Herz SL, Ingrassia CM, Costa KD, Holmes JW, Homma S, Laine AF. Region-based endocardium tracking on real-time three-dimensional ultrasound. Ultrasound Med Biol 2008;35: 256–265.

Elen A, Choi HF, Loeckx D, Gao H, Claus P, Suetens P, Maes F, D'Hooge J. Three-dimensional cardiac strain estimation using spatio-temporal elastic registration of ultrasound images: A feasibility study. IEEE Trans Med Imaging 2008;27:1580–1591.

Georgescu B, Zhou XS, Comaniciu D, Gupta A. Database-guided segmentation of anatomical structures with complex appearance. Proc IEEE Conf Comput Vis Pattern Recogn 2005;2:429–436.

Gérard O, Billon AC, Rouet JM, Jacob M, Fradkin M, Allouche C. Efficient model-based quantification of left ventricular function in 3-D echocardiography. IEEE Trans Med Imaging 2002;21:1059–1068.

Gower JC. Generalized Procrustes analysis. Psychometrika 1975;40: 33–51.

Hansegård J, Orderud F, Rabben SI. Real-time active shape models for segmentation of 3D cardiac ultrasound. Proc Comput Anal Images Patt, LNCS 4673 2007a;157–164.

Hansegård J, Urheim S, Lunde K, Rabben SI. Constrained active appearance models for segmentation of triplane echocardiograms. IEEE Trans Med Imaging 2007b;26:1391–1400.

Helle-Valle T, Crosby J, Edvardsen T, Lyseggen E, Amundsen BH, Smith HJ, Rosen BD, Lima JA, Torp H, Ihlen H, Smiseth OA. New noninvasive method for assessment of left ventricular rotation: Speckle tracking echocardiography. Circulation 2005;112: 3149–3156.

Horn BKP, Schunck BG. Determining optical flow. Artif Intell 1981;17: 185–203.

Kawagishi T. Speckle tracking for assessment of cardiac motion and dyssynchrony. Echocardiography 2008;25:1167–1171.

Ledesma-Carbayo MJ, Kybic J, Desco M, Santos A, Sühling M, Hunziker P, Unser M. Spatio-temporal nonrigid registration for ultrasound cardiac motion estimation. IEEE Trans Med Imaging 2005;24:1113–1126.

Leung KYE, Bosch JG. Segmental wall motion classification in echocardiograms using compact shape descriptors. Acad Radiol 2008; 15:1416–1424.

Leung KYE, Bosch JG. Automated border detection in 3D echocardiography– Principles and promises. Eur J Echocardiogr 2010;11: 97–108.

Leung KYE, Van Stralen M, Nemes A, Voormolen MM, Van Burken G, Geleijnse ML, Ten Cate FJ, Reiber JHC, Van der Steen AFW, De Jong N, Bosch JG. Sparse registration for three-dimensional stress echocardiography. IEEE Trans Med Imaging 2008;27: 1568–1579.

Leung KYE, van Stralen M, van Burken G, de Jong N, Bosch JG. Automatic active appearance model segmentation of 3D echocardiograms. Proc Int Symp Biomed Imaging 2010;320–323.

Lin N, Yu W, Duncan JS. Combinative multi-scale level set framework for echocardiographic image segmentation. Med Image Anal 2003; 7:529–537.

Linguraru MG, Vasilyev NV, Marx GR, Tworetzky W, Del Nido PJ, Howe RD. Fast block flow tracking of atrial septal defects in 4D echocardiography. Med Image Anal 2008;12:397–412.

Lucas BD, Kanade T. An iterative image registration technique with an application to stereo vision. Proc DARPA Image Understanding Workshop 1981;121–130.

Mailloux GE, Bleau A, Bertrand M, Petitclerc R. Computer analysis of heart motion from two-dimensional echocardiograms. IEEE Trans Bio Med Eng 1987;34:356–364.

Malassiotis S, Strintzis MG. Tracking the left ventricle in echocardiographic images by learning heart dynamics. IEEE Trans Med Imaging 1999;18:282–290.

Malpica N, Santos A, Zuluaga MA, Ledesma MJ, Pérez E, García-Fernández MA, Desco M. Tracking of regions-of-interest in myocardial contrast echocardiography. Ultrasound Med Biol 2004;30: 303–309.

Mikić I, Krucinski S, Thomas JD. Segmentation and tracking in echocardiographic sequences: Active contours guided by optical flow estimates. IEEE Trans Med Imaging 1998;17:274–284.

Mitchell SC, Bosch JG, Lelieveldt BPF, van der Geest RJ, Reiber JHC, Sonka M. 3-D active appearance models: Segmentation of cardiac MR and ultrasound images. IEEE Trans Med Imaging 2002;21: 1167–1178.

Montagnat J, Sermesant M, Delingette H, Malandain G, Ayache N. Anisotropic filtering for model-based segmentation of 4D cylindrical echocardiographic images. Pattern Recogn Lett 2003;24: 815–828.

Myronenko A, Song X, Sahn DJ. LV motion tracking from 3D echocardiography using textural and structural information. Proc Med Image Comput Comput Assist Interv, LNCS 4792 2007;428–435.

Nemes A, Geleijnse ML, Krenning BJ, Soliman OII, Anwar AM, Vletter WB, ten Cate FJ. Usefulness of ultrasound contrast agent to improve image quality during real-time three-dimensional stress echocardiography. Am J Cardiol 2007;99:275–278.

Nillesen MM, Lopata RGP, Gerrits IH, Kapusta L, Huisman HJ, Thijssen JM, de Korte CL. Segmentation of the heart muscle in 3-D pediatric echocardiographic images. Ultrasound Med Biol 2007;33:1453–1462.

Noble JA, Boukerroui D. Ultrasound image segmentation: A survey. IEEE Trans Med Imaging 2006;25:987–1010.

Orderud F, Hansegård J, Rabben SI. Real-time tracking of the left ventricle in 3D echocardiography using a state estimation approach. Proc Med Image Comput Comput Assist Interv, LNCS 4791 2007;858–865.

Papademetris X, Sinusas AJ, Dione DP, Duncan JS. Estimation of 3D left ventricular deformation from echocardiography. Med Image Anal 2001;5:17–28.

Perperidis D, Mohiaddin R, Edwards P, Rueckert D. Segmentation of cardiac MR and CT image sequences using model based registration of a 4D statistical model. Proc SPIE Med Imaging 2007;6512: 65121D.

Sanchez-Ortiz GI, Wright GJT, Clarke N, Declerck J, Banning AP, Noble JA. Automated 3-D echocardiography analysis compared with manual delineations and SPECT MUGA. IEEE Trans Med Imaging 2002;21:1069–1076.

Sühling M, Arigovindan M, Jansen C, Hunziker P, Unser M. Myocardial motion analysis from B-mode echocardiograms. IEEE Trans Image Process 2005;14:525–536.

Van Ginneken B, Stegmann MB, Loog M. Segmentation of anatomical structures in chest radiographs using supervised methods: A comparative study on a public database. Med Image Anal 2006;10:19–40.

van Stralen M, Bosch JG, Voormolen MM, van Burken G, Krenning BJ, van Geuns RM, Lancée CT, de Jong N, Reiber JH. Left ventricular volume estimation in cardiac three-dimensional ultrasound: A semi-automatic border detection approach. Acad Radiol 2005;12: 1241–1249.

van Stralen M, Leung KYE, Voormolen MM, de Jong N, van der Steen AFW, Reiber JHC, Bosch JG. Automatic segmentation of the left ventricle in 3D echocardiography using active appearance models. Proc IEEE Int Ultrason Symp 2007;1480–1483.

Veronesi F, Corsi C, Caiani EG, Sarti A, Lamberti C. Tracking of left ventricular long axis from real-time three-dimensional echocardiography using optical flow techniques. IEEE Trans Inf Technol Biomed 2006;10:174–181.

Walimbe V, Zagrodsky V, Shekhar R. Fully automatic segmentation of left ventricular myocardium in real-time three-dimensional echocardiography. Proc SPIE Med Imaging 2006;6144:61444H.

Wolf I, Hastenteufel M, De Simone R, Vetter M, Glombitza G, Mottl-Link S, Vahl CF, Meinzer HP. ROPES: A semiautomated segmentation method for accelerated analysis of three-dimensional echocardiographic data. IEEE Trans Med Imaging 2002;21: 1091–1104.

Yan P, Sinusas A, Duncan JS. Boundary element method-based regularization for recovering of LV deformation. Med Image Anal 2007; 11:540–554.

Yang L, Georgescu B, Zheng Y, Foran DJ, Comaniciu D. A fast and accurate tracking algorithm of left ventricles in 3D echocardiography. Proc Int Symp Biomed Imaging 2008;221–224.

Yeung F, Levinson SF, Parker KJ. Multilevel and motion model-based ultrasonic speckle tracking algorithms. Ultrasound Med Biol 1998; 24:427–441.

Zagrodsky V, Walimbe V, Castro-Pareja CR, Qin JX, Song JM, Shekhar R. Registration-assisted segmentation of real-time 3-D echocardiographic data using deformable models. IEEE Trans Med Imaging 2005;24:1089–1099.

Zhu Y, Papademetris X, Sinusas A, Duncan JS. Segmentation of myocardial volumes from real-time 3D echocardiography using an incompressibility constraint. Proc Med Image Comput Comput Assist Interv, LNCS 4791 2007;44–51.